inorganics

MDPI

Article

Preliminary Characterization of a Ni^{2+}-Activated and Mycothiol-Dependent Glyoxalase I Enzyme from *Streptomyces coelicolor*

Uthaiwan Suttisansanee [1,2] and John F. Honek [1,*]

[1] Department of Chemistry, University of Waterloo, 200 University Avenue West, Waterloo, ON N2L 3G1, Canada

[2] Institute of Nutrition, Mahidol University, 25/25 Phutthamonthon 4 Rd., Salaya, Phutthamonthon, Nakhon Pathom 73170, Thailand

* Correspondence: jhonek@uwaterloo.ca; Tel.: +1-1519-888-4567 (ext. 35817)

Received: 6 July 2019; Accepted: 9 August 2019; Published: 14 August 2019

Abstract: The glyoxalase system consists of two enzymes, glyoxalase I (Glo1) and glyoxalase II (Glo2), and converts a hemithioacetal substrate formed between a cytotoxic alpha-ketoaldehyde, such as methylglyoxal (MG), and an intracellular thiol, such as glutathione, to a non-toxic alpha-hydroxy acid, such as D-lactate, and the regenerated thiol. Two classes of Glo1 have been identified. The first is a Zn^{2+}-activated class and is exemplified by the *Homo sapiens* Glo1. The second class is a Ni^{2+}-activated enzyme and is exemplified by the *Escherichia coli* Glo1. Glutathione is the intracellular thiol employed by Glo1 from both these sources. However, many organisms employ other intracellular thiols. These include trypanothione, bacillithiol, and mycothiol. The trypanothione-dependent Glo1 from *Leishmania major* has been shown to be Ni^{2+}-activated. Genetic studies on *Bacillus subtilis* and *Corynebacterium glutamicum* focused on MG resistance have indicated the likely existence of Glo1 enzymes employing bacillithiol or mycothiol respectively, although no protein characterizations have been reported. The current investigation provides a preliminary characterization of an isolated mycothiol-dependent Glo1 from *Streptomyces coelicolor*. The enzyme has been determined to display a Ni^{2+}-activation profile and indicates that Ni^{2+}-activated Glo1 are indeed widespread in nature regardless of the intracellular thiol employed by an organism.

Keywords: glyoxalase; nickel; streptomyces; mycothiol; metalloenzyme

1. Introduction

Intracellularly generated cytotoxic alpha-ketoaldehydes, such as methylglyoxal (MG; Figure 1), are highly reactive electrophiles that can inhibit protein synthesis, form adducts with protein, DNA and RNA, and promote Advanced Glycation End-products (AGEs) [1–8]. Detoxification of these molecules is a critical cellular process. The enzymes Glyoxalase I (Glo1) and Glyoxalase II (Glo2) work in tandem and convert the hemithioacetal, formed between the cytotoxic α-ketoaldehyde and an intracellular thiol, such as glutathione (GSH), into a non-toxic alpha-hydroxy acid, such as D-lactate (in the case of MG), and the regenerated thiol (Figure 1) [9–13]. Reduction of cellular toxicity is also dependent upon *S*-lactoylglutathione levels as this product of the Glo1 reaction can also control bacterial potassium efflux pumps and cytosolic acidification [14]. The metalloenzyme Glo1 catalyzes the isomerization reaction resulting in the production of the thioester product. Hydrolysis of the thioester is catalyzed by the second metalloenzyme, Glo2. An additional type of glyoxalase enzyme, Glo3, utilizes an active site cysteine to convert MG to D-lactate directly [15–18].

Glo1 is a metalloenzyme that can be divided into two different metal-activation classes [19]. The Zn^{2+}-activated class is exemplified by the enzyme from *Homo sapiens* (homodimeric), and the

Ni^{2+}-activated Glo1 class is exemplified by the enzyme from *Escherichia coli* (homodimeric) [20–25]. In the case of the *E. coli* enzyme, the Ni^{2+}-active form (Protein Database (PDB): 1F9Z) is situated in an octahedral ligand arrangement (residues from chain A: His5 and Glu56; residues from chain B: His74 and Glu122) with two water molecules as non-proteinaceous ligands, but the inactive Zn^{2+}-bound complex (PDB: 1FA5) has a trigonal bipyramidal ligand arrangement and has only one water molecule as a non-proteinaceous ligand (Figure 2) [26,27]. A similar octahedral ligand arrangement (residues from chain A: Gln34 and Glu100; residues from chain B: His127 and Glu173) is observed for the catalytically active Zn^{2+}-bound form of the *H. sapiens* Glo1 (PDBN: 1QIN) [28,29]. Thus, only octahedral metal environments appear to be active for this enzyme, regardless of the metal-activation class the Glo1 belongs to, and this arrangement appears critical to the enzyme's catalytic mechanism [30–32].

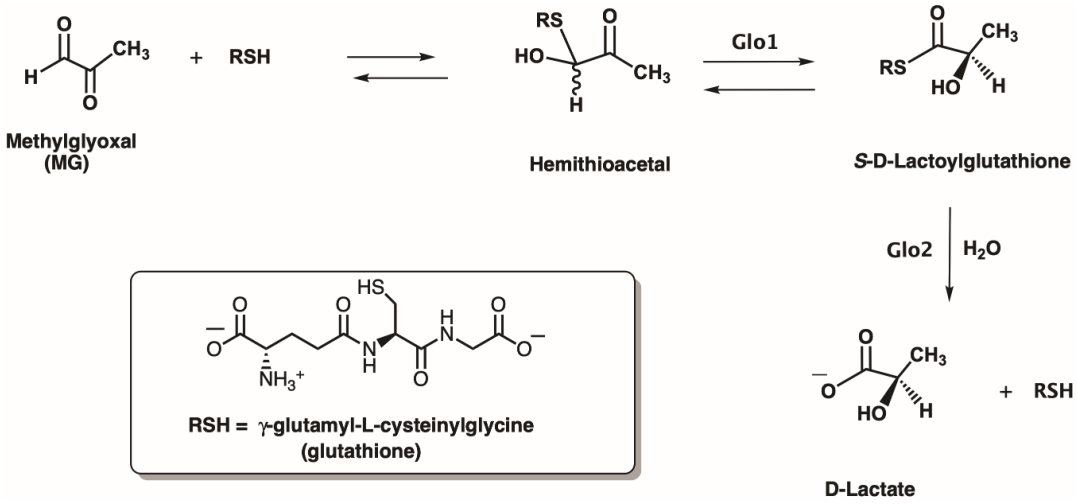

Figure 1. The overall reaction of the enzymes glyoxalase I (Glo1) and glyoxalase II (Glo2). The intracellular thiol utilized in many, but not all, organisms is the tripeptide glutathione.

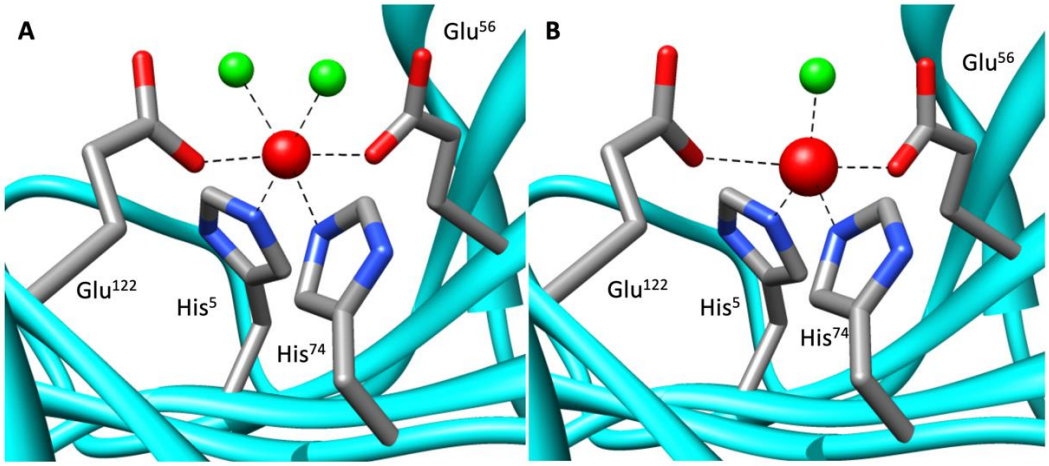

Figure 2. The ribbon structure of (**A**) the active Ni^{2+}-bound *Escherichia coli* Glo1 (PDB ID: 1F9Z) forming an octahedral geometry with four metal-binding residues (His^5, Glu^{56}, His^{74} and Glu^{122}) and two nearby water molecules around the metal center and (**B**) the inactive Zn^{2+}-bound *E. coli* Glo1 (PDB ID: 1FA5) forming a trigonal bipyramidal metal coordination with the same four metal-binding residues but with only one water molecule [27]. The metal-binding residues are shown in sticks, and active site water molecules are shown in green. The divalent metals in the catalytic pocket are represented as red spheres. The 3D structures were generated by using the UCSF Chimera program (University of California, San Francisco, CA, USA) [33].

Structural studies have been reported on several Glo1, and these reports have provided additional insight into nature's control of active site geometry. As mentioned, the *H. sapiens* and *E. coli* enzymes are homodimeric, and each of their two active sites is formed by residues contributed by each of the two subunits. The molecular structure of the *Clostridium acetobutylicum* Glo1 (Ni^{2+}-activation class) is also homodimeric, but each of the two active sites is formed by protein residues solely from a *single* subunit [34]. Furthermore, larger single chain Glo1 are also known [35–41], and the recent report on the X-ray structure of the maize enzyme shows two metal-binding sites formed by the single protein chain with one site being catalytically active [42]. For the homodimeric Glo1, as well as the maize enzyme, detailed studies employing metal activation, NMR and X-ray experiments have provided unambiguous evidence that only a single active site is required for maximal activity [42–44]. In addition, deletional mutagenesis experiments have recently provided insight into the underlying structural factors involved in metal selectivity among the Glo1 enzymes [45].

To further add to the complex but fascinating biochemistry of Glo1, it has become clear that Glo1 enzymes have evolved to employ whatever major intracellular thiol [46–50] is available to them within a particular organism (Figure 3). In addition to glutathione (GSH), which is present in eukaryotes and most Gram-negative bacteria, protozoans, such as *Leishmania* and *Trypanosoma* employ N^1,N^8-bis (L-γ-glutamyl-L-hemicystinyl-glycyl) spermidine, trypanothione, for their cellular biochemistry, which includes their Glo1 enzymes [51–53]. The *Leishmania major* Glo1 has been determined to be a Ni^{2+}-activated class enzyme and lacks catalytic activity with Zn^{2+} [51,54]. The Glo1 from *Trypanosoma cruzi* has also been determined to be Ni^{2+}-activated enzymes [55]. The intracellular thiol, (2*S*)-2-[[2-(L-cysteinylamino)-2-deoxy-α-D-glucopyranosyl]oxy]succinic acid, known as bacillithiol (Figure 3), is present in bacilli, such as *Bacillus subtilis* and *B. anthracis,* and has also been identified in *Staphylococcus aureus,* as well as *Deinococcus radiodurans* [49,56–59]. Genetic studies on *Bacillus subtilis* have indicated the likely existence of a Glo1 enzyme employing bacillithiol, although no reports on the isolation and characterization of a bacillithiol-dependent Glo1 have been reported [60].

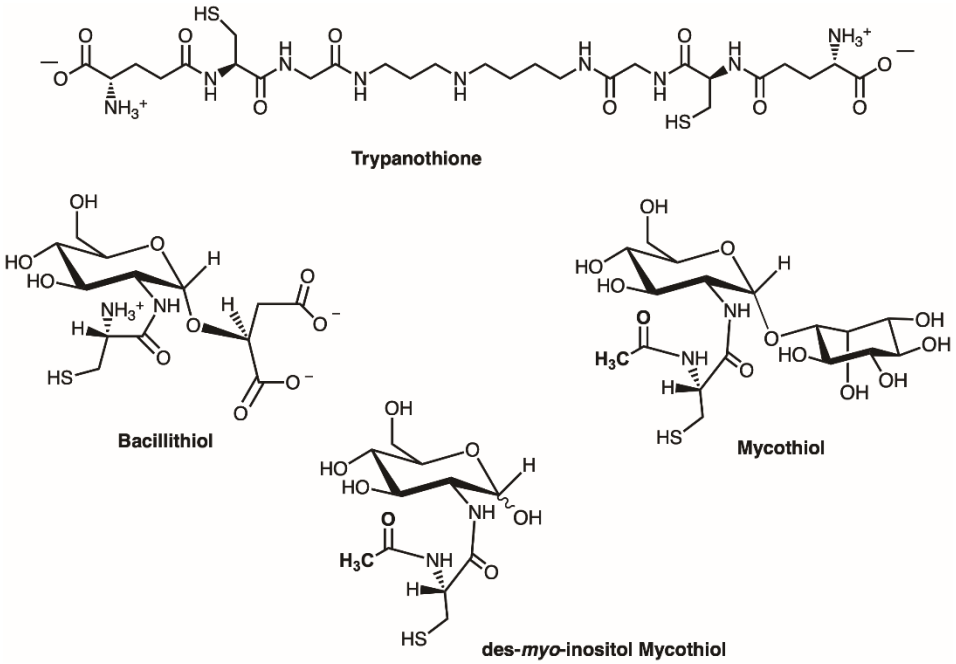

Figure 3. Several important intracellular thiols found in nature (trypanothione, bacillithiol, mycothiol). Des-*myo*-inositol mycothiol (tMSH) is an analog of mycothiol also employed in the current study.

Actinomycetes and mycobacteria biosynthesize the thiol, 1-D-myo-inositol-2-(*N*-acetyl-L-cysteinyl) amido-2-deoxy-α-D-glucopyranoside, mycothiol (Figure 3) [61–64]. Although substantial information is now available on the biochemical pathways employing mycothiol, and the functions of mycothiol and

its metabolic pathways appear to parallel those of glutathione, to date no reports have appeared on the characterization of a mycothiol-dependent Glo1. However, mycothiol-null mutants in *Corynebacterium glutamicum* have been reported to endow this organism with MG sensitivity, indicating the possible existence of a mycothiol-dependent Glo1 [63].

In order to extend our knowledge of the Glo1 metalloenzymes, an investigation was undertaken to identify and provide a preliminary characterization of a mycothiol-dependent Glo1 (Figure 4), if it indeed existed. The current investigation reports on the identification of such an enzyme in *Streptomyces coelicolor* and provides a preliminary characterization of the isolated Glo1. The Glo1 from *Streptomyces coelicolor* has been determined to exhibit a homodimeric quaternary structure and to be a member of the Ni^{2+}-activation class of glyoxalase I enzymes.

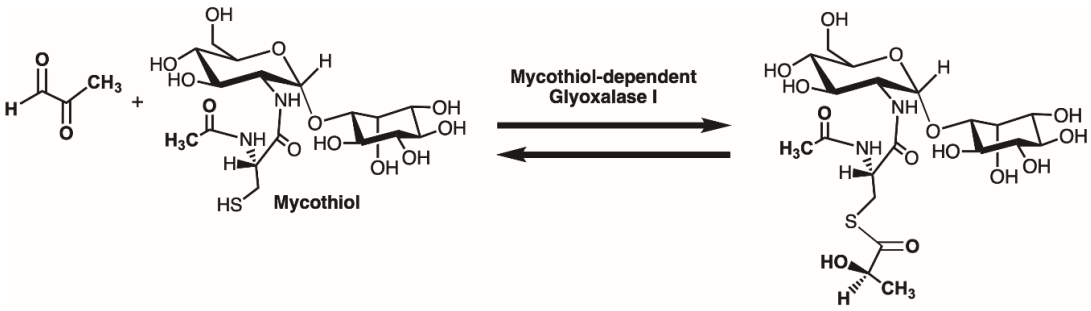

Figure 4. The overall reaction of a mycothiol-dependent glyoxalase I enzyme.

2. Results and Discussion

2.1. Sequence Analysis

As mycothiol is the key intracellular thiol in Streptomyces, sequence searching of a number of sequence databases, including the Streptomyces Annotation Server (http://streptrdb.streptomyces.org.uk), for a possible Glo1 enzyme employing various known Glo1 sequences was undertaken for the organism Streptomyces coelicolor A3(2) [65,66]. The search revealed two genes of interest with annotations of a putative dioxygenase/glyoxalase/ bleomycin resistance family gene product (SCO1970; EMBLCAC42744; NCBI reference sequence: NP_626233.1), which was termed putative dioxygenase (PDO), and a putative lyase (SCO2237; EMBLCAC37263; NCBI reference sequence: NP_626487.1), which was termed putative lyase (PLA). Multiple sequence alignments of PDO and PLA with other Glo1 from various sources, including Gram-negative bacteria (*E. coli* [24], *Yersinia pestis* [19], *Neisseria meningitides* [19,67], *Pseudomonas aeruginosa* GloA2 [68], *P. aeruginosa* GloA3 [68], and *P. putida* [22]), protozoa (*Leishmania major* [51]), human (*H. sapiens* [23]), and the previously identified gene [60] correlated with possible bacillithiol-dependent Glo1 activity in Bacillus subtilis are shown in Figure 5. In this group, the known metal-specificities of the Glo1 are as follows: Zn^{2+}-dependent (*P. putida*, *H. sapiens*, *P. aeruginosa* GloA3) and Ni^{2+}-dependent (*E. coli*, *Y. pestis*, *N. meningitidis*, *P. aeruginosa* GloA2, *L. major*). The metal specificity of the *B. subtilis* enzyme is unknown as the protein has not been isolated nor characterized. PDO possesses four potential metal-binding residues (His^{15}, Asp^{63}, His^{89}, Glu^{142}) corresponding to metal-binding residue positions in other Glo1 enzymes (astericks in Figure 5). The corresponding residues in PLA (Val^{7}, Asp^{62}, Tyr^{75}, Gln^{127}) do not map as well, and the alignment suggests that PDO would be the more likely candidate to demonstrate Glo1 activity, although both gene products were investigated. Based on the alignment, PDO has a 21.7% identity and 20.2% identity to the *N. meningitidis* Glo1 and the *B. subtilis* gene product associated with the bacillithiol-dependent Glo1 activity, respectively (Figure S1). Based on previous sequence alignments and deletional mutagenesis experiments, it has been suggested that shorter Glo1 sequences tend to be Ni^{2+}-activated class enzymes [19]. In the case of PDO, if indeed a Glo1, a Ni^{2+}-activated class enzyme was hypothesized.

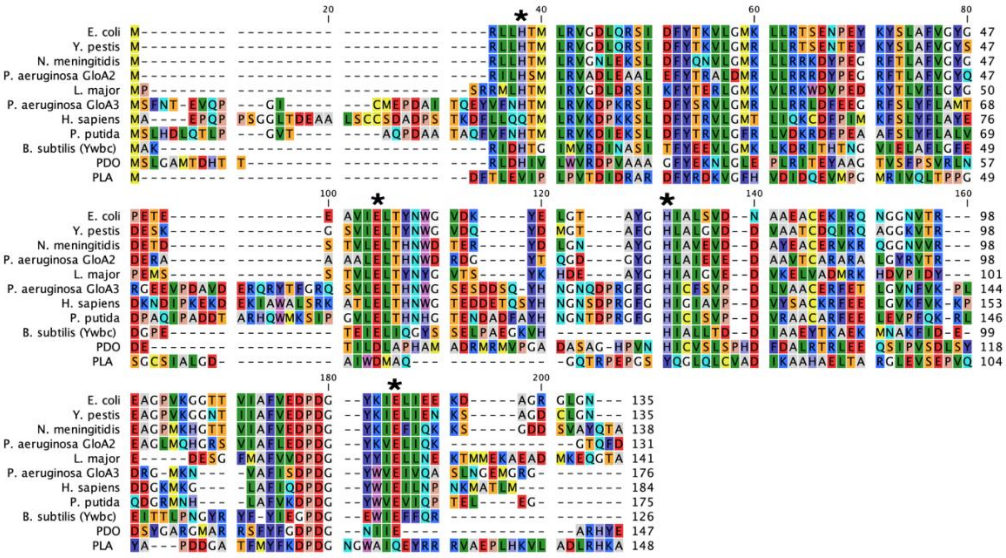

Figure 5. The multiple sequence alignment of the putative dioxygenase (PDO, CAC42744) and the putative lyase (PLA, CAC37263) from Streptomyces coelicolor A3(2) with glyoxalase I from other organisms (organism name followed by National Center for Biotechnology Information (NCBI) accession number), including *E. coli* (NP_310387), *Y. pestis* (ZP_01887743.1), *N. meningitides* (CAA74673), *P. aeruginosa* GloA2 (ATE47122.1), *L. major* (AAT98624.1), *P. aeruginosa* GloA3 (AAG08496.1), *H. sapiens* (AAB49495), *P. putida* (AAN69360), *B. subtilis* bacillithiol-dependent MG resistance proposed Glo1 (P39586.1). The metal-binding residues are highlighted with asterisks. Three different Glo1 have been identified in *P. aeruginosa* PA01: GloA1 (Ni^{2+}-activated), GloA2 (Ni^{2+}-activated and GloA3 (Zn^{2+}-activated) [68]. The alignment was created using CLC Main Workbench (version 8.1.2) with the accurate alignment algorithm (http://www.qiagenbioinformatics.com).

2.2. Overproduction, Isolation and Characterization of PDO and PLA

The putative dioxygenase gene (*pdo*) and putative lyase gene (*pla*) from chromosomal DNA from *S. coelicolor* A3(2) (NC_003888) were cloned into pET-28b(+) expression vectors utilizing NdeI and BamHI restriction endonuclease enzymes and polymerase chain reaction (PCR) to generate the purified proteins with an N-terminal His-tag followed by a thrombin protease cleavage site. The protein purification of PDO and PLA made use of the N-terminal His-tag, which was eventually removed by thrombin protease, resulting in three extra amino acids at the N-terminus (Gly-Ser-His) fused to the N-terminal Met residues. These modifications changed the predicted molecular weights of PDO and PLA to 16569.5 Da and 16749.9 Da, respectively, which were confirmed by electrospray ionization mass spectrometry (ESI-MS) analysis (Figures S2 and S3). No post-translational modification of either purified protein was observed. Analysis of a gel permeation chromatographic separation suggested a homodimeric quaternary structure for both PDO (1.5 mg mL^{-1}) and PLA (0.6 mg mL^{-1}) in 50 mM Tris (pH 8.0) and 150 mM KCl with a molecular weight of approximately 27.51 ± 2.46 kDa and 33.15 ± 2.89 kDa, respectively (Figure S4). The thermal stabilities of PDO and PLA as isolated were performed using differential scanning calorimetry (DSC) analysis, which suggested the estimated T_m of PDO (3 mg mL^{-1}) and PLA (1.2 mg mL^{-1}) in 50 mM MOPS (pH 7.0) and 10% *v*/*v* glycerol to be 57.8 and 58.5 °C, respectively (Figure S5). Their secondary structures were investigated by circular dichroism (CD) analysis which showed that both PDO (5.6 mg mL^{-1}) and PLA (3.6 mg mL^{-1}) in buffer containing 50 mM potassium phosphate buffer (KPB; pH 7.0) and 200 mM KCl possessed a negative maximum at 222 nm and a small shoulder at 208 nm, suggesting the presence of predominantly β-sheet structures (Figure S6), which are consistent with the previous reports on the X-ray crystallographic structures of other Glo1. The K2D3 secondary structural prediction program (http://cbdm-01.zdv.uni-mainz.de/~{}andrade/k2d3/) also estimated the secondary structural contents of PDO to be 1–2% α-helix, 37–41% β-sheet and 58–62% random coil and of PLA to be 2–6% α-helix, 34–40% β-sheet and 57–62% random coil. Other external

factors, including pH (5–9), types of buffer (HEPES, KPB, Tris, MOPS and MOPSO), ionic strength (0–500 mM NaCl) and additive (0–30% *v*/*v* glycerol) did not significantly influence the secondary structures of either protein (data not shown).

2.3. Enzyme Assay for Thiol Cofactors

Optimization of the Glo1 enzyme assays employed the simpler and more readily available [69] truncated form of mycothiol (tMSH; des-myo-inositol mycothiol) (Figure 3) [70]. This analog has been employed in the study of mycothiol-utilizing enzymes [71]. Mycothiol was also employed at various stages in this study, especially with respect to final enzyme kinetic studies [70]. Experiments to study the details of the non-enzymatic formation of the hemithioacetal upon MG and tMSH reaction in solution were undertaken initially and included enzyme kinetic assays and ^{1}H NMR time course studies, benchmarked to previously studied MG and glutathione adduct formation studies (Figures S7–S10 and Tables S1 and S2) [24,72–79]. Analysis of the results of these experiments indicated that a 30 min equilibration time would be appropriate for the MG-tMSH hemithioacetal equilibrium to be attained, a time somewhat longer than that for the equilibrium to be reached for the MG-GSH hemithioacetal equilibrium to be reached (15 min).

The dissociation constant (K_d) of the hemithioacetal (MG-tSH) was also determined, due to its significance in the calculation of the exact concentration of the substrate used in the Glo1 kinetic assays. After allowing the hemithioacetal to reach its equilibrium (15 min for MG-GSH and 30 min for MG-tMSH), the dissociation constant could be measured using different concentrations of MG with a fixed concentration of thiols, an approach previously employed in the literature for MG-GSH [24,72–77]. The dissociation profile of MG-GSH suggested its K_d of approximately 3.19 ± 0.29 mM (Figure S10A), which was in excellent agreement to the literature value (K_d of 3.1 mM). The K_d of the hemithioacetal forming non-enzymatically between MG and tMSH was determined similarly and estimated to be 3.33 ± 0.41 mM (Figure S10B).

The increase in UV absorbance at 240 nm observed during the reaction of Glo1 is due to the formation of the product, *S*-D-lactolyglutathione, from the Glo1 reaction using MG-GSH as a substrate. The investigation on the optimum detection wavelength for the reaction using MG-tMSH substrate was performed similarly, and the results suggested that the detection at 240 nm could also be employed to detect the thioester product from the MG-tMSH substrate (Figure S11). Furthermore, the expected product, *S*-D-lactoyl-des-myo-inositol mycothiol, produced from the Glo1 catalyzed reaction using Ni^{2+}-reconstituted PDO (25 µg in 600 µL assay) with MG-tMSH (5 mM, K_d of 3.3 mM and equilibrium time of 30 min), was isolated using reverse phase C18 HPLC (Figure S12) and was identified by ESI-MS analysis (Figure S13), consistent with PDO serving as a mycothiol-dependent Glo1. It should be noted however that although the mass of the product is consistent with the chemical structure of the expected product, the exact determination of the stereochemistry of the lactate as D-lactate has not been shown, although it is highly likely given the commonality of the stereochemistry found in the product from various Glo1 enzymes.

Based on the information obtained on hemithioacetal formation as stated above, the substrate specificity of the Glo1 reaction was investigated in relation to metal-incorporation and the presence of PDO, PLA or commercial yeast Glo1 (1.5–3.0 µg for PDO and PLA and 0.05 µg for yeast Glo1 in 200 µL assay). The detection of the substrates, including MG, GSH, tMSH, hemithioacetal of MG-GSH and hemithioacetal of MG-tMSH did not show any significant increase in signal at 240 nm without the corresponding enzyme. Neither was product formation detected for any of these substrates in the presence of added metal ions (without the addition of the enzyme), suggesting that substrates with and without additional metal ions do not interfere with the detection of the enzyme reaction, if any—nor do they contribute any significant non-enzyme background activity. No Glo1 activity was observed for reactions containing only MG, only GSH, only tMSH, or only MG-GSH with Ni^{2+}-reconstituted PDO. Neither were any reactions observed to occur in the reactions of apo-PDO and denatured PDO (boiled for 10 min) with hemiacetal MG-tMSH. However, trace activity was obtained in the reaction of isolated

PDO (purified PDO without any additional metals) with MG-tMSH, while high activity was observed in the reaction of Ni^{2+}-reconstituted PDO with the same substrate. These observations suggested that the incorporated metal into PDO is significant for the Glo1 reaction to occur and that the "as isolated" PDO is not entirely in its apo-form, and this was confirmed by inductively coupled mass spectrometry (ICP-MS) analysis for the presence of metal ions in the PDO protein (Table S3). The isolated PDO enzyme might accept some metals from the organism's growth environment during the expression and purification processes undertaken in the laboratory. Additionally, the reaction catalyzed by the PDO enzyme is specific to the hemithioacetal substrate, MG-tMSH, while the substrate of the GSH-dependent Glo1 reaction, MG-GSH (5 mM), did not act as a substrate for PDO (data not shown). PLA, on the other hand, did not exhibit any glutathione or tMSH-dependent Glo1 activity under the above conditions. The enzymatic reaction catalyzed by yeast Glo1 is specific to its substrate, MG-GSH, in which it was observed to exhibit no activity in the presence of the MG-tMSH hemithioacetal.

2.4. Metal Characterization and Kinetic Studies

The metal analysis determined by ICP-MS (ALS Laboratory Group, Waterloo, ON, Canada), undertaken utilizing protocols [24,25,34,45,68] previously employed, suggested that the purified "as isolated" (no exogenously added metal ions) PDO (0.088 mg/mL) binds to copper, cobalt, nickel and zinc ions (Tables S3 and S4). The metal per enzyme ratios of nickel-and zinc-bound PDO were approximately 0.16–0.17, while those of cobalt and copper-bound enzyme were approx. 0.02. Thus, the ratios of Ni^{2+} and Zn^{2+} contents were approximately ten times higher than those of Co^{2+} and Cu^{2+}, which might suggest that PDO has a higher metal-binding affinity for Ni^{2+} and Zn^{2+} than Co^{2+} and Cu^{2+} ions, or could reflect the availability of these metal ions in *E. coli* during protein production and isolation steps. The concentrations of these incorporated metals in the isolated protein were low and appeared almost completely in a de-metallated form. The ICP-MS analysis on this form of the PDO indicated that the enzyme contained no iron, a common metal found in dioxygenase enzymes, but it did contain ions, such as zinc and nickel bound to the isolate protein. Both Zn^{2+} and Ni^{2+}, as previously mentioned, are metals that are usually associated with Glo1 enzymes. These results suggest that PDO may bind either of these metals in intact *S. coelicolor*, although, of course, these metals could have been picked up by the protein in steps associated with the protein isolation.

Analysis of the metal activation profile for PDO suggested that the enzyme was activated in the presence of Ni^{2+}, Cu^{2+}, and to a much lower extent by Cd^{2+} and Ca^{2+} (activity of PDO: $Ni^{2+} > Cu^{2+} > Cd^{2+} > Ca^{2+}$) (Figure 6A). The enzyme with incorporated Ni^{2+} exhibited the highest activity of conversion of the MG-tMSH hemithioacetal into its thioester, while that of Cu^{2+}-reconstitution gave approximately 60% compared to that of the Ni^{2+}-reconstituted enzyme. The activities with Cd^{2+} and Ca^{2+}-were low, while other metal ions (Zn^{2+}, Mg^{2+}, Co^{2+}, Mn^{2+}) were not activating. Metal titration studies of PDO with Ni^{2+} and Cu^{2+} indicated that 1 mole of metal per mole dimeric enzyme could optimize enzymatic activity (Figure 6B), suggesting a tight binding of the metal, as well as one functional active site (possibly two active sites per dimeric enzyme as PDO exhibits homodimeric quaternary structure as previously mentioned). These data are consistent with previous reports on other Glo1 (such as *E. coli* Glo1, *P. aeruginosa* GloA1, GloA2, and many others), which also find that the metal per dimeric enzyme ratio is approximately one [19,24,44,68]. The pH dependency of PDO activity was also determined (Figure 6C).

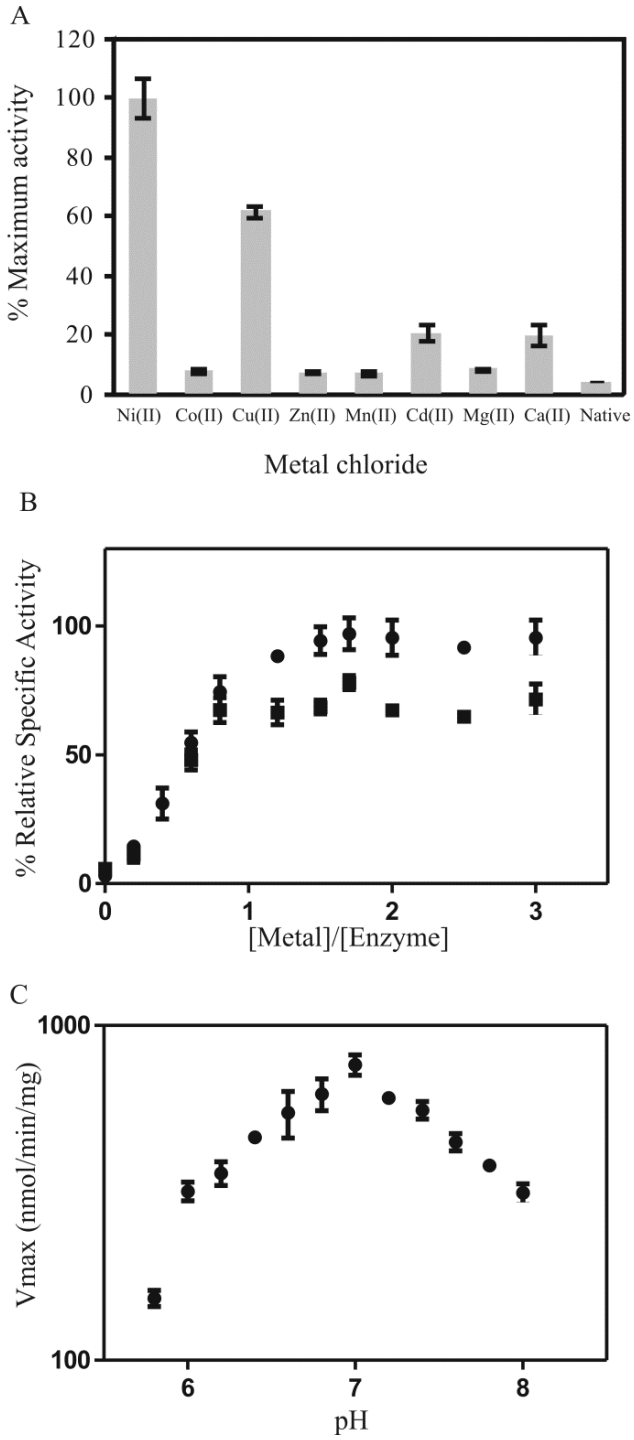

Figure 6. (**A**) PDO metal activation profile after metal ion (5 equivalents) preincubation of the apo-form of the enzyme with metal chloride (conditions: PDO (3.1 μg in 200 μL) incubated with metal chlorides overnight at 4 °C); (**B**) % Relative specific enzyme activity of PDO versus metal ion titration with (●) Ni^{2+} and (■) Cu^{2+}; (**C**) pH dependency of PDO (3.125 μg in 200 μL assay; 5 equivalents $NiCl_2$) with the substrate MG-tMSH (0.5 mM, K_d = 3.3 mM) that was incubated for 30 min in potassium phosphate buffer at various pH (5.8–8) at 25 °C.

The kinetics of Ni^{2+}-reconstituted PDO with MG-tMSH yielded a calculated V_{max} of 5.8 ± 1.0 μmol/min/mg, K_m of 1.25 ± 0.13 mM and k_{cat} of 3.2 s^{-1} (Table 1). The K_m is somewhat higher compared to other K_m values for the MG-GSH substrate processed by other Glo1 [24,34,68,80,81],

which is probably due to the structure of the MG-tMSH hemithioacetal lacking the inositol moiety. This hypothesis was confirmed by the kinetics of Ni^{2+}-reconstituted PDO with the hemithioacetal of MG-MSH which yielded a calculated V_{max} of 11.5 ± 1.8 µmol/min/mg, K_m of 0.61 ± 0.06 mM and k_{cat} of 6.4 s^{-1} (Table 1).

Table 1. Kinetic data for the enzyme reaction catalyzed by Ni^{2+}-reconstituted PDO.

Thiol Cofactors	V_{max} (µmol/min/mg)	K_m (µM)	k_{cat} (s^{-1})	k_{cat}/K_m ($M^{-1}s^{-1}$)
MSH	11.5 ± 1.8	612 ± 56	6.4	10403
tMSH	5.8 ± 1.0	1247 ± 127	3.2	2545

Conditions: PDO (1.5–3.0 µg in 200 µL assay) using two different hemithioacetal substrates (0.08–1 mM, K_d = 3.3 mM, 30 min equilibrium time) that formed non-enzymatically between methylglyoxal and thiol cofactors, including isolated mycothiol (MSH) and synthesized truncated mycothiol (tMSH), in 50 mM KPB (pH 6.6) at 25 °C. The protein was prepared in its apo-form and incubated with five equivalents of $NiCl_2$ overnight at 4 °C prior to performing the assay.

Metal analysis performed on the "as isolated" PLA exhibited similar results, where copper, nickel and zinc were detected bound to various copies of the protein (Tables S3 and S5). The metal per dimeric enzyme ratios of nickel-and zinc-bound PLA were approx. 0.11–0.16, while the ratio of copper bound enzyme was 0.08. The concentrations of these metals were low, which indicated that PLA is isolated in predominantly apo-form. Glo1 activity of PLA, on the other hand, was undetectable under the studied conditions. The enzyme exhibited no activity with MG-tMSH nor MG-GSH (data not shown). Neither activity was observed in the presence of different divalent metals ($ZnCl_2$, $NiCl_2$, $CoCl_2$, $CuCl_2$, $MnCl_2$, $MgCl_2$, $CaCl_2$ and $CdCl_2$), suggesting that PLA does not function as a Glo1.

Glo1 is a member of the βαββββ superfamily of proteins, consisting of fosfomycin resistance protein (FosA), methylmalonyl-CoA epimerase (MMCE), extradiol dioxygenase (DIOX), mitomycin C resistance protein (MRP) and bleomycin resistance protein (BRP) [23,34,40,82–88]. Among these proteins, Glo1 and MMCE share high structural similarity, thiol cofactor (GSH), presence of divalent metal and tetradentated metal-binding protein ligands [34,85]. Due to these similarities, an investigation of possible MMCE activity in PDO and PLA with selected incorporated metals (Ni^{2+}, Co^{2+}, Cu^{2+}, and Zn^{2+}) was performed, similar to those previously reported for studies on the *C. acetobutylicum* Glo1 [34]. Ni^{2+}, Co^{2+} and Zn^{2+} are activating metal ions for particular Glo1 enzymes, while Co^{2+} is normally found in MMCE enzymes. Cu^{2+} was also chosen for our studies, due to its observed activation of PDO in the Glo1 reaction with Mg-tMSH. However, neither enzyme exhibited any MMCE activity understudied conditions (data not shown), and no divalent metal could activate these enzymes to accomplish the MMCE activity. Thus, PDO only functions as a Glo1 and not as an MMCE, while PLA is neither a Glo1 nor an MMCE. Previous investigations on the MMCE activity in GSH-dependent Glo1 from Clostridium acetobutylicum suggest that the enzyme is highly specific to its natural substrate (MG-GSH) even though its structure is more likely to resemble that of MMCE than other Glo1 [34]. These results suggest that Glo1 does not possess cross function with MMCE regardless of its different types of thiol cofactors that might be used across nature.

PDO is activated with Ni^{2+} and Cu^{2+} atoms. The unusual metal activation by Cu^{2+} in PDO may be anomalous and not related to any physiological role of this metal in the organism. However, it is interesting to speculate that it may be an important metal for this enzyme in the organism, since cytosolic copper has been found to be a major modulator of *Streptomyces coelicolor* germination, development and secondary metabolism [89]. It is also interesting to note that mycothiol has been found to be important in copper resistance in *C. glutamicum* [63], and perhaps there may be an advantage to mycothiol-dependent Glo1 to be able to utilize Cu^{2+} as an activating metal. However, this requires further research to confirm or dispute.

It had been found earlier that the isolated mammalian GloI exhibited high activity in the presence of Mg^{2+} and was thought to be a magnesium activated enzyme [21,90–92]. However, the naturally bound metal was later discovered to be zinc, which incorporated in the ratio of 1 mole metal per mole enzyme subunit [20]. The magnesium atoms were believed to be recovered from protein preparation

processes and had no correlation with enzymatic activity. The analysis by electron paramagnetic resonance (EPR) of Co^{2+}-bound human Glo1, however, suggested octahedral metal coordination with four metal-binding protein residues and two water molecules for this ion, as well as other activating metals, such as magnesium [29]. Yeast Glo1 was also found to be partially activated by the presence of Mg^{2+} and Ca^{2+} [20,36,93]. It was possible that these metals could reactivate the enzyme, but play a major role in protein stability. As well, X-ray crystallographic structure of *E. coli* Glo1 with bound Cd^{2+} (PDB ID: 1FA7) suggested that the enzyme could be activated with this metal and its metal coordination forms an octahedral geometry [27]. However, the activity was low compared to the enzyme with Ni^{2+} and Co^{2+}, which might be related to the size of the metal that fits into the active site of the enzyme. Thus, the low activity observed in PDO with Ca^{2+} and Cd^{2+} might be explained in a similar fashion.

It is hoped that this preliminary characterization of a mycothiol-dependent Glo1 will provide important information for future studies on Glo1 enzymes from other microorganisms employing mycothiol, as well as bacillithiol, a closely related intracellular thiol.

3. Materials and Methods

3.1. DNA Cloning and Manipulation

All DNA manipulations and purifications were performed according to the protocols by Sambrook and Russell [94]. Putative dioxygenase gene (*pdo*) and putative lyase gene (*pla*) from *S. coelicolor* chromosome (NC_003888) were cloned into the pET-28b(+) expression vector utilizing *Nde*I and *BamH*I restriction endonuclease enzymes and the polymerase chain reaction (PCR) to generate the protein with the N-terminal His-tag followed by thrombin protease cleavage site. The forward and reverse primers (Sigma Genosys, Oakville, Ontario, Canada) were designed as follows: (+) 5′-CCGAAGCTTCATATGAGCCTGGGAGCC-3′ and (−) 5′-GGCGAATTCGGATCC TACTCGTAGTG CCGG-3′ for *pdo* cloning, and (+) 5′-CCGAAGCTTCATATGGACTTCACGCTCG-3′ and (−) 5′-GGCGAATTCGGATCCTAGGCCTTGTGCCGG-3′ for *pla* cloning. The plasmid was heat shock transformed into the competent *E. coli* DH5α cells. Its DNA sequence was verified (Molecular Biology Core Facility, University of Waterloo, Waterloo, ON, USA) followed by heat shock transforming into *E. coli* BL21 (DE3) cells for protein expression purposes. Sequence alignments and percent identities were computed using CLC Main Workbench (version 8.1.2) (http://www.qiagenbioinformatics.com).

3.2. Protein Induction, Expression, and Purification

Bacterial cultures (1 L) containing kanamycin (30 μg/mL LB) were grown and shaken in an air incubator (220 rpm) at 37 °C until an OD_{600} of 0.6 was reached. Proteins were then induced with 0.5 mM IPTG for 4 h. Cell pellets were harvested by centrifugation at 6000× *g* for 10 min and flash frozen in liquid nitrogen before storing at −80 °C. The purifications of both PDO and PLA were performed as previously reported for the *C. acetobutylicum* Glo1 [34] using HisTrap HP Ni^{2+}-affinity (1 mL) and HiTrap Benzamidine FF affinity (1 mL) columns (GE Healthcare, Piscataway, NJ, USA). The protein concentration was determined by the Bradford Assay using bovine serum albumin (BSA) as a standard. Apo-enzyme preparation and metal analysis by ICP-MS were performed as described previously for other Glo1 and other enzymes [25,95–97]. The existence and the molecular weights of the denatured proteins were confirmed by the analysis of SDS-PAGE and ESI-MS data using a Micromass Q-TOF Global Ultima mass spectrometer (Mass Spectrometry Facility, University of Waterloo, Waterloo, ON, USA) using handling approaches as previously reported [68,78]. The molecular weight of the native protein was determined by gel permeation chromatography (Superose6 10/300 GL column) utilizing 50 mM Tris buffer (pH 8.0) and 150 mM KCl with a flow rate of 0.5 mL/min. A standard curve was prepared using Bio-Rad protein standards (Bio-Rad Laboratories, Hercules, CA, USA) containing γ-globulin (158 kDa), BSA (66 kDa), ovalbumin (44 kDa), carbonic anhydrase (29 kDa), myoglobulin (17 kDa) and vitamin B_{12} (1.35 kDa).

3.3. Protein Secondary Structure and Stability Experiments

CD experiments were performed on a Jasco J-715 spectropolarimeter from Jasco Inc. (Easton, MD, USA) and a Jasco J-700 Standard Analysis Program. The CD experiments with variation in protein concentration, pH, ionic strength and various additives were performed as previously reported. Prediction of protein secondary structure from CD spectra employed the K2D3 program as previously mentioned [98]. The transition midpoint (T_m) determined by DSC analysis was performed on a MicroCal VP-DSC microcalorimeter with cell volumes of 0.5 mL and self-contained pressurizing system of 0–30 p.s.i. for scanning solutions above boiling points to prevent any degassing during heating. The protein was run against 50 mM MOPS (pH 7.0) and 10% *v/v* glycerol over a temperature range of 10–80 °C with a scanning rate of 1 °C min^{-1}. The Origin, scientific plotting software package, supplied by MicroCal was used for baseline subtraction and T_m calculation by the integration of the heat capacity (C_p) versus temperature (t) curve.

3.4. Preparation of Hemithioacetal Substrate

tMSH was synthesized according to the protocol developed by Unson et al. [70]. Purified MSH was a kind gift from Dr. Gerald Newton (UCSD, San Diego, CA, USA) [70]. Two factors involved in the hemithioacetal substrate formation, including equilibrium time and dissociation constant (K_d) of MG-GSH, were previously reported, but none for MG-tMSH and MG-MSH. We assumed that the hemithioacetal formations of MG-tMSH and MG-MSH were in a similar fashion, thus only equilibrium time and K_d of MG-tMSH were determined as detailed in the Supplementary Materials using the protocols reported for MG-GSH. ^{1}H NMR experiments were performed on a Bruker (300 MHz) spectrometer (Bruker Ltd., Milton, ON, Canada). Predicted chemical shifts and integrations for substrates and hemithioacetals were estimated using ChemBioDraw Ultra 12.0 (http://www.cambridgesoft.com) software (version 12.0, PerkinElmer, Austin, TX, USA).

3.5. Enzyme Assays

An enzymatic assay was performed in 50 mM KPB (pH 6.6 or stated otherwise) using the hemithioacetal, a non-enzymatic product of MG and thiol cofactors (GSH, tMSH and MSH), as substrates utilizing previous Glo1 assay protocols [24,78]. The enzyme activity was measured as an increase in absorption at 240 nm (ε_{240} = 2860 M^{-1} cm^{-1}) for the formation of *S*-D-lactoylglutathione using a 96-well UV-visible plate on a plate reader. Since the product of the mycothiol dependent Glo1 reaction is unknown, its maximum absorbance and identification were investigated to confirm the existence of the reaction product thioester (Supplementary Materials). Enzyme kinetics were evaluated using the initial rate that was fitted by the Michaelis-Menten equation with least squares fit parameters using GraphPad Prism software version 5.00 (GraphPad Software, Inc., La Jolla, CA, USA). Typical conditions for Glo1 activity studies on PDO were: PDO (1.5–3.0 µg in 200 µL assay) using two different hemithioacetal substrates (0.08–1 mM, K_d = 3.3 mM, 30 min equilibrium time) that formed non-enzymatically between methylglyoxal and thiol cofactors, including isolated MSH and tMSH, in 50 mM KPB (pH 6.6) at 25 °C. The protein was prepared in its apo-form and incubated with five equivalents of $NiCl_2$ overnight at 4 °C prior to performing the assay.

Additionally, the investigation on the function of MMCE, a closely structural related protein to Glo1 in the same βαββββ superfamily, was performed using metal-substituted PDO and PLA (1 µg in 500 µL assay) in 20 mM Tris (pH 7.0) and 150 mM NaCl with the presence of 5 equivalents of Ni^{2+}, Co^{2+}, Cu^{2+} and Zn^{2+} as previously described for another Glo1 enzyme study [34].

4. Conclusions

Identification and isolation of a glyoxalase I (Glo1) enzyme from *Streptomyces coelicolor* A3(2) was accomplished in this study. A preliminary investigation of several properties of the protein, termed PDO (thermal stability, pH dependency on activity, secondary structure) was undertaken. PDO was

found to be catalytically active as a glyoxalase I enzyme in the presence of Ni^{2+}, and converted the hemithioacetals formed from methylglyoxal and des-*myo*-inositol mycothiol (tMSH) to the identified thioester product. No enzymatic activity was observed using glutathione, suggesting PDO is specific to tMSH and after further experimentation, mycothiol itself. From the metal activation profile, PDO functions as a mycothiol-dependent Glo1 of the Ni^{2+}-activated class of glyoxalase I enzymes. This is the first protein characterization of an MSH-dependent Glo1.

Supplementary Materials: The following are available online at http://www.mdpi.com/2304-6740/7/8/99/s1, Figure S1: Percent identities calculated for various Glo1, Figure S2: SDS-PAGE and ESI mass spectrum of purified PDO, Figure S3: SDS-PAGE and ESI mass spectrum of purified PLA, Figure S4: Gel permeation chromatographic profile for PDO and PLA, Figure S5: DSC plots for PDO and PLA, Figure S6: CD plots for PDO and PLA, Figure S7: Enzymatic assay using various incubation times, Figure S8: ^{1}H NMR for various time incubations of MG and GSH, Table S1: Chemical Shifts and Integrations of 1H NMR signals (experimental and calculated) for GSH and MG-GSH, Figure S9: ^{1}H NMR for various time incubations of MG and tMSH, Table S2: Chemical Shifts and Integrations of 1H NMR signals (experimental and calculated) for tMSH and MG-tMSH, Figure S10: Plots for the determination of *Kd* for MG-GSH and MG-tMSH hemithioacetals, Figure S11: UV detection of MG-tMSH thioester product, Figure S12: HPLC chromatogram of products of MG-tMSH Glo1 activity by PDO, Figure S13: ESI mass spectrum of isolated thioester product, Table S3–S5: ICP-MS element analyses of "as isolated" PDO and PLA.

Author Contributions: Conceptualization: J.F.H.; Investigation and draft writing: U.S. and J.F.H.; writing—review and editing: J.F.H. and U.S.

Funding: This research was funded by NSERC (Canada) (JH) and the University of Waterloo (JH), and the Government of Thailand for a graduate scholarship (US).

Acknowledgments: The authors would like to thank Richard Smith for electrospray ionization MS analysis of the protein sample, Elisabeth Daub for *Streptomycetes* handling and David Ward, Michele Cossette and Vincent Azhikannickal for support of tMSH synthesis and enzyme purification. As well, we thank Zhengding Su, Christine Hand and Nicole Sukdeo for sharing their knowledge and suggestions. Gerard Wright (McMaster University) is gratefully acknowledged for supplying the *Streptomyces coelicolor* A3(2) strain. The authors gratefully acknowledge Gerald Newton (University of California Sand Diego) for the kind gift of purified mycothiol used in this investigation.

Conflicts of Interest: The authors declare no conflict of interest. The funders had no role in the design of the study; in the collection, analyses, or interpretation of data; in the writing of the manuscript, or in the decision to publish the results.

References

1. Thornalley, P.J. Dietary AGEs and ALEs and risk to human health by their interaction with the receptor for advanced glycation endproducts (RAGE)—An introduction. *Mol. Nutr. Food Res.* **2007**, *51*, 1107–1110. [CrossRef] [PubMed]
2. Krautwald, M.; Munch, G. Advanced glycation end products as biomarkers and gerontotoxins—A basis to explore methylglyoxal-lowering agents for Alzheimer's disease? *Exp. Gerontol.* **2010**, *45*, 744–751. [CrossRef] [PubMed]
3. Rabbani, N.; Thornalley, P.J. Dicarbonyl stress in cell and tissue dysfunction contributing to ageing and disease. *Biochem. Biophys. Res. Commun.* **2015**, *458*, 221–226. [CrossRef] [PubMed]
4. Schalkwijk, C.G. Vascular AGE-ing by methylglyoxal: The past, the present and the future. *Diabetologia* **2015**, *58*, 1715–1719. [CrossRef] [PubMed]
5. Honek, J.F. Glyoxalase biochemistry. *Biomol. Concepts* **2015**, *6*, 401–414. [CrossRef] [PubMed]
6. Thornalley, P.J. Protein and nucleotide damage by glyoxal and methylglyoxal in physiological systems—Role in ageing and disease. *Drug Metabol. Drug Interact.* **2008**, *23*, 125–150. [CrossRef] [PubMed]
7. Trellu, S.; Courties, A.; Jaisson, S.; Gorisse, L.; Gillery, P.; Kerdine-Romer, S.; Vaamonde-Garcia, C.; Houard, X.; Ekhirch, F.P.; Sautet, A.; et al. Impairment of glyoxalase-1, an advanced glycation end-product detoxifying enzyme, induced by inflammation in age-related osteoarthritis. *Arthritis Res. Ther.* **2019**, *21*, 18. [CrossRef] [PubMed]
8. De Bari, L.; Atlante, A.; Armeni, T.; Kalapos, M.P. Synthesis and metabolism of methylglyoxal, *S*-D-lactoylglutathione and D-lactate in cancer and Alzheimer's disease. Exploring the crossroad of eternal youth and premature aging. *Ageing Res. Rev.* **2019**, *53*, 100915. [CrossRef] [PubMed]

9. Sousa Silva, M.; Gomes, R.A.; Ferreira, A.E.; Ponces Freire, A.; Cordeiro, C. The glyoxalase pathway: The first hundred years... and beyond. *Biochem. J.* **2013**, *453*, 1–15. [CrossRef] [PubMed]
10. Sukdeo, N.; Honek, J.F. Microbial glyoxalase enzymes: Metalloenzymes controlling cellular levels of methylglyoxal. *Drug Metabol. Drug Interact.* **2008**, *23*, 29–50. [CrossRef]
11. Rabbani, N.; Xue, M.; Thornalley, P.J. Dicarbonyls and glyoxalase in disease mechanisms and clinical therapeutics. *Glycoconj. J.* **2016**, *33*, 513–525. [CrossRef] [PubMed]
12. Rabbani, N.; Thornalley, P.J. Glyoxalase Centennial conference: Introduction, history of research on the glyoxalase system and future prospects. *Biochem. Soc. Trans.* **2014**, *42*, 413–418. [CrossRef] [PubMed]
13. Thornalley, P.J. Glyoxalase I—Structure, function and a critical role in the enzymatic defence against glycation. *Biochem. Soc. Trans.* **2003**, *31*, 1343–1348. [CrossRef] [PubMed]
14. Ozyamak, E.; Black, S.S.; Walker, C.A.; Maclean, M.J.; Bartlett, W.; Miller, S.; Booth, I.R. The critical role of S-lactoylglutathione formation during methylglyoxal detoxification in *Escherichia coli*. *Mol. Microbiol.* **2010**, *78*, 1577–1590. [CrossRef] [PubMed]
15. Misra, K.; Banerjee, A.B.; Ray, S.; Ray, M. Glyoxalase III from *Escherichia coli*: A single novel enzyme for the conversion of methylglyoxal into D-lactate without reduced glutathione. *Biochem. J.* **1995**, *305 Pt 3*, 999–1003. [CrossRef]
16. Choi, D.; Kim, J.; Ha, S.; Kwon, K.; Kim, E.H.; Lee, H.Y.; Ryu, K.S.; Park, C. Stereospecific mechanism of DJ-1 glyoxalases inferred from their hemithioacetal-containing crystal structures. *FEBS J.* **2014**, *281*, 5447–5462. [CrossRef] [PubMed]
17. Zhao, Q.; Su, Y.; Wang, Z.; Chen, C.; Wu, T.; Huang, Y. Identification of glutathione (GSH)-independent glyoxalase III from *Schizosaccharomyces pombe*. *BMC Evol. Biol.* **2014**, *14*, 86. [CrossRef] [PubMed]
18. Subedi, K.P.; Choi, D.; Kim, I.; Min, B.; Park, C. Hsp31 of *Escherichia coli* K-12 is glyoxalase III. *Mol. Microbiol.* **2011**, *81*, 926–936. [CrossRef] [PubMed]
19. Sukdeo, N.; Clugston, S.L.; Daub, E.; Honek, J.F. Distinct classes of glyoxalase I: Metal specificity of the *Yersinia pestis*, *Pseudomonas aeruginosa* and *Neisseria meningitidis* enzymes. *Biochem. J.* **2004**, *384*, 111–117. [CrossRef]
20. Aronsson, A.C.; Marmstal, E.; Mannervik, B. Glyoxalase I, a zinc metalloenzyme of mammals and yeast. *Biochem. Biophys. Res. Commun.* **1978**, *81*, 1235–1240. [CrossRef]
21. Han, L.P.; Schimandle, C.M.; Davison, L.M.; Vander Jagt, D.L. Comparative kinetics of Mg^{2+}-, Mn^{2+}-, Co^{2+}-, and Ni^{2+}-activated glyoxalase I. Evaluation of the role of the metal ion. *Biochemistry* **1977**, *16*, 5478–5484. [CrossRef] [PubMed]
22. Saint-Jean, A.P.; Phillips, K.R.; Creighton, D.J.; Stone, M.J. Active monomeric and dimeric forms of *Pseudomonas putida* glyoxalase I: Evidence for 3D domain swapping. *Biochemistry* **1998**, *37*, 10345–10353. [CrossRef] [PubMed]
23. Cameron, A.D.; Olin, B.; Ridderstrom, M.; Mannervik, B.; Jones, T.A. Crystal structure of human glyoxalase I—Evidence for gene duplication and 3D domain swapping. *EMBO J.* **1997**, *16*, 3386–3395. [CrossRef] [PubMed]
24. Clugston, S.L.; Barnard, J.F.; Kinach, R.; Miedema, D.; Ruman, R.; Daub, E.; Honek, J.F. Overproduction and characterization of a dimeric non-zinc glyoxalase I from *Escherichia coli*: Evidence for optimal activation by nickel ions. *Biochemistry* **1998**, *37*, 8754–8763. [CrossRef] [PubMed]
25. Clugston, S.L.; Yajima, R.; Honek, J.F. Investigation of metal binding and activation of *Escherichia coli* glyoxalase I: Kinetic, thermodynamic and mutagenesis studies. *Biochem. J.* **2004**, *377*, 309–316. [CrossRef] [PubMed]
26. Davidson, G.; Clugston, S.L.; Honek, J.F.; Maroney, M.J. XAS investigation of the nickel active site structure in *Escherichia coli* glyoxalase I. *Inorg. Chem.* **2000**, *39*, 2962–2963. [CrossRef] [PubMed]
27. He, M.M.; Clugston, S.L.; Honek, J.F.; Matthews, B.W. Determination of the structure of *Escherichia coli* glyoxalase I suggests a structural basis for differential metal activation. *Biochemistry* **2000**, *39*, 8719–8727. [CrossRef] [PubMed]
28. Cameron, A.D.; Ridderstrom, M.; Olin, B.; Kavarana, M.J.; Creighton, D.J.; Mannervik, B. Reaction mechanism of glyoxalase I explored by an X-ray crystallographic analysis of the human enzyme in complex with a transition state analogue. *Biochemistry* **1999**, *38*, 13480–13490. [CrossRef]
29. Sellin, S.; Eriksson, L.E.; Aronsson, A.C.; Mannervik, B. Octahedral metal coordination in the active site of glyoxalase I as evidenced by the properties of Co(II)-glyoxalase I. *J. Biol. Chem.* **1983**, *258*, 2091–2093.

30. Himo, F.; Siegbahn, P.E. Catalytic mechanism of glyoxalase I: A theoretical study. *J. Am. Chem. Soc.* **2001**, *123*, 10280–10289. [CrossRef]
31. Richter, U.; Krauss, M. Active site structure and mechanism of human glyoxalase I—An ab initio theoretical study. *J. Am. Chem. Soc.* **2001**, *123*, 6973–6982. [CrossRef] [PubMed]
32. Davidson, G.; Clugston, S.L.; Honek, J.F.; Maroney, M.J. An XAS investigation of product and inhibitor complexes of Ni-containing GlxI from *Escherichia coli*: Mechanistic implications. *Biochemistry* **2001**, *40*, 4569–4582. [CrossRef] [PubMed]
33. Pettersen, E.F.; Goddard, T.D.; Huang, C.C.; Couch, G.S.; Greenblatt, D.M.; Meng, E.C.; Ferrin, T.E. UCSF Chimera—A visualization system for exploratory research and analysis. *J. Comput. Chem.* **2004**, *25*, 1605–1612. [CrossRef] [PubMed]
34. Suttisansanee, U.; Lau, K.; Lagishetty, S.; Rao, K.N.; Swaminathan, S.; Sauder, J.M.; Burley, S.K.; Honek, J.F. Structural variation in bacterial glyoxalase I enzymes: Investigation of the metalloenzyme glyoxalase I from *Clostridium acetobutylicum*. *J. Biol. Chem.* **2011**, *286*, 38367–38374. [CrossRef] [PubMed]
35. Deponte, M.; Sturm, N.; Mittler, S.; Harner, M.; Mack, H.; Becker, K. Allosteric coupling of two different functional active sites in monomeric *Plasmodium falciparum* glyoxalase I. *J. Biol. Chem.* **2007**, *282*, 28419–28430. [CrossRef] [PubMed]
36. Frickel, E.M.; Jemth, P.; Widersten, M.; Mannervik, B. Yeast glyoxalase I is a monomeric enzyme with two active sites. *J. Biol. Chem.* **2001**, *276*, 1845–1849. [CrossRef] [PubMed]
37. Inoue, Y.; Maeta, K.; Nomura, W. Glyoxalase system in yeasts: Structure, function, and physiology. *Semin. Cell Dev. Biol.* **2011**, *22*, 278–284. [CrossRef] [PubMed]
38. Iozef, R.; Rahlfs, S.; Chang, T.; Schirmer, H.; Becker, K. Glyoxalase I of the malarial parasite *Plasmodium falciparum*: Evidence for subunit fusion. *FEBS Lett.* **2003**, *554*, 284–288. [CrossRef]
39. Turra, G.L.; Agostini, R.B.; Fauguel, C.M.; Presello, D.A.; Andreo, C.S.; Gonzalez, J.M.; Campos-Bermudez, V.A. Structure of the novel monomeric glyoxalase I from *Zea mays*. *Acta Crystallogr. D Biol. Crystallogr.* **2015**, *71*, 2009–2020. [CrossRef]
40. Kaur, C.; Vishnoi, A.; Ariyadasa, T.U.; Bhattacharya, A.; Singla-Pareek, S.L.; Sopory, S.K. Episodes of horizontal gene-transfer and gene-fusion led to co-existence of different metal-ion specific glyoxalase I. *Sci. Rep.* **2013**, *3*, 3076. [CrossRef]
41. Mustafiz, A.; Ghosh, A.; Tripathi, A.K.; Kaur, C.; Ganguly, A.K.; Bhavesh, N.S.; Tripathi, J.K.; Pareek, A.; Sopory, S.K.; Singla-Pareek, S.L. A unique Ni^{2+} -dependent and methylglyoxal-inducible rice glyoxalase I possesses a single active site and functions in abiotic stress response. *Plant J.* **2014**, *78*, 951–963. [CrossRef]
42. Gonzalez, J.M.; Agostini, R.B.; Alvarez, C.E.; Klinke, S.; Andreo, C.S.; Campos-Bermudez, V.A. Deciphering the number and location of active sites in the monomeric glyoxalase I of *Zea mays*. *FEBS J.* **2019**. [CrossRef]
43. Su, Z.; Sukdeo, N.; Honek, J.F. 15N-1H HSQC NMR evidence for distinct specificity of two active sites in *Escherichia coli* glyoxalase I. *Biochemistry* **2008**, *47*, 13232–13241. [CrossRef]
44. Bythell-Douglas, R.; Suttisansanee, U.; Flematti, G.R.; Challenor, M.; Lee, M.; Panjikar, S.; Honek, J.F.; Bond, C.S. The crystal structure of a homodimeric *Pseudomonas* glyoxalase I enzyme reveals asymmetric metallation commensurate with half-of-sites activity. *Chemistry* **2015**, *21*, 541–544. [CrossRef]
45. Suttisansanee, U.; Ran, Y.; Mullings, K.Y.; Sukdeo, N.; Honek, J.F. Modulating glyoxalase I metal selectivity by deletional mutagenesis: Underlying structural factors contributing to nickel activation profiles. *Metallomics* **2015**, *7*, 605–612. [CrossRef]
46. Hand, C.E.; Honek, J.F. Biological chemistry of naturally occurring thiols of microbial and marine origin. *J. Nat. Prod.* **2005**, *68*, 293–308. [CrossRef]
47. Wang, M.; Zhao, Q.; Liu, W. The versatile low-molecular-weight thiols: Beyond cell protection. *Bioessays* **2015**, *37*, 1262–1267. [CrossRef]
48. Newton, G.L.; Arnold, K.; Price, M.S.; Sherrill, C.; Delcardayre, S.B.; Aharonowitz, Y.; Cohen, G.; Davies, J.; Fahey, R.C.; Davis, C. Distribution of thiols in microorganisms: Mycothiol is a major thiol in most actinomycetes. *J. Bacteriol.* **1996**, *178*, 1990–1995. [CrossRef]
49. Gaballa, A.; Newton, G.L.; Antelmann, H.; Parsonage, D.; Upton, H.; Rawat, M.; Claiborne, A.; Fahey, R.C.; Helmann, J.D. Biosynthesis and functions of bacillithiol, a major low-molecular-weight thiol in Bacilli. *Proc. Natl. Acad. Sci. USA* **2010**, *107*, 6482–6486. [CrossRef]
50. Jothivasan, V.K.; Hamilton, C.J. Mycothiol: Synthesis, biosynthesis and biological functions of the major low molecular weight thiol in actinomycetes. *Nat. Prod. Rep.* **2008**, *25*, 1091–1117. [CrossRef]

51. Vickers, T.J.; Greig, N.; Fairlamb, A.H. A trypanothione-dependent glyoxalase I with a prokaryotic ancestry in *Leishmania major*. *Proc. Natl. Acad. Sci. USA* **2004**, *101*, 13186–13191. [CrossRef]
52. Oza, S.L.; Shaw, M.P.; Wyllie, S.; Fairlamb, A.H. Trypanothione biosynthesis in *Leishmania major*. *Mol. Biochem. Parasitol.* **2005**, *139*, 107–116. [CrossRef]
53. Greig, N.; Wyllie, S.; Patterson, S.; Fairlamb, A.H. A comparative study of methylglyoxal metabolism in trypanosomatids. *FEBS J.* **2009**, *276*, 376–386. [CrossRef]
54. Ariza, A.; Vickers, T.J.; Greig, N.; Armour, K.A.; Dixon, M.J.; Eggleston, I.M.; Fairlamb, A.H.; Bond, C.S. Specificity of the trypanothione-dependent *Leishmania major* glyoxalase I: Structure and biochemical comparison with the human enzyme. *Mol. Microbiol.* **2006**, *59*, 1239–1248. [CrossRef]
55. Greig, N.; Wyllie, S.; Vickers, T.J.; Fairlamb, A.H. Trypanothione-dependent glyoxalase I in *Trypanosoma cruzi*. *Biochem. J.* **2006**, *400*, 217–223. [CrossRef]
56. Fahey, R.C. Glutathione analogs in prokaryotes. *Biochim. Biophys. Acta* **2013**, *1830*, 3182–3198. [CrossRef]
57. Sharma, S.V.; Arbach, M.; Roberts, A.A.; Macdonald, C.J.; Groom, M.; Hamilton, C.J. Biophysical features of bacillithiol, the glutathione surrogate of *Bacillus subtilis* and other firmicutes. *ChemBioChem* **2013**, *14*, 2160–2168. [CrossRef]
58. Perera, V.R.; Newton, G.L.; Pogliano, K. Bacillithiol: A key protective thiol in *Staphylococcus aureus*. *Expert Rev. Anti Infect. Ther.* **2015**, *13*, 1089–1107. [CrossRef]
59. Chandrangsu, P.; Loi, V.V.; Antelmann, H.; Helmann, J.D. The Role of Bacillithiol in Gram-Positive Firmicutes. *Antioxid. Redox Signal.* **2018**, *28*, 445–462. [CrossRef]
60. Chandrangsu, P.; Dusi, R.; Hamilton, C.J.; Helmann, J.D. Methylglyoxal resistance in *Bacillus subtilis*: Contributions of bacillithiol-dependent and independent pathways. *Mol. Microbiol.* **2014**, *91*, 706–715. [CrossRef]
61. Sao Emani, C.; Williams, M.J.; Wiid, I.J.; Baker, B. The functional interplay of low molecular weight thiols in *Mycobacterium tuberculosis*. *J. Biomed. Sci.* **2018**, *25*, 55. [CrossRef]
62. Sharma, S.V.; Van Laer, K.; Messens, J.; Hamilton, C.J. Thiol Redox and pKa Properties of Mycothiol, the Predominant Low-Molecular-Weight Thiol Cofactor in the Actinomycetes. *ChemBioChem* **2016**, *17*, 1689–1692. [CrossRef]
63. Liu, Y.B.; Long, M.X.; Yin, Y.J.; Si, M.R.; Zhang, L.; Lu, Z.Q.; Wang, Y.; Shen, X.H. Physiological roles of mycothiol in detoxification and tolerance to multiple poisonous chemicals in *Corynebacterium glutamicum*. *Arch. Microbiol.* **2013**, *195*, 419–429. [CrossRef]
64. Newton, G.L.; Buchmeier, N.; Fahey, R.C. Biosynthesis and functions of mycothiol, the unique protective thiol of Actinobacteria. *Microbiol. Mol. Biol. Rev.* **2008**, *72*, 471–494. [CrossRef]
65. Bentley, S.D.; Chater, K.F.; Cerdeno-Tarraga, A.M.; Challis, G.L.; Thomson, N.R.; James, K.D.; Harris, D.E.; Quail, M.A.; Kieser, H.; Harper, D.; et al. Complete genome sequence of the model actinomycete *Streptomyces coelicolor* A3(2). *Nature* **2002**, *417*, 141–147. [CrossRef]
66. Park, J.H.; Cha, C.J.; Roe, J.H. Identification of genes for mycothiol biosynthesis in *Streptomyces coelicolor* A3(2). *J. Microbiol.* **2006**, *44*, 121–125.
67. Kizil, G.; Wilks, K.; Wells, D.; Ala'Aldeen, D.A. Detection and characterisation of the genes encoding glyoxalase I and II from *Neisseria meningitidis*. *J. Med. Microbiol.* **2000**, *49*, 669–673. [CrossRef]
68. Sukdeo, N.; Honek, J.F. *Pseudomonas aeruginosa* contains multiple glyoxalase I-encoding genes from both metal activation classes. *Biochim. Biophys. Acta* **2007**, *1774*, 756–763. [CrossRef]
69. Hamilton, C.J.; Finlay, R.M.; Stewart, M.J.; Bonner, A. Mycothiol disulfide reductase: A continuous assay for slow time-dependent inhibitors. *Anal. Biochem.* **2009**, *388*, 91–96. [CrossRef]
70. Unson, M.D.; Newton, G.L.; Davis, C.; Fahey, R.C. An immunoassay for the detection and quantitative determination of mycothiol. *J. Immunol. Methods* **1998**, *214*, 29–39. [CrossRef]
71. Patel, M.P.; Blanchard, J.S. Synthesis of des-myo-inositol mycothiol and demonstration of a mycobacterial specific reductase activity. *J. Am. Chem. Soc.* **1998**, *120*, 11538–11539. [CrossRef]
72. Vander Jagt, D.L.; Han, L.P.; Lehman, C.H. Kinetic evaluation of substrate specificity in the glyoxalase-I-catalyzed disproportionation of α-ketoaldehydes. *Biochemistry* **1972**, *11*, 3735–3740. [CrossRef]
73. Vince, R.; Daluge, S.; Wadd, W.B. Studies on the inhibition of glyoxalase I by S-substituted glutathiones. *J. Med. Chem.* **1971**, *14*, 402–404. [CrossRef]
74. Cliffe, E.E.; Waley, S.G. The mechanism of the glyoxalase I reaction, and the effect of ophthalmic acid as an inhibitor. *Biochem. J.* **1961**, *79*, 475–482. [CrossRef]

75. Creighton, D.J.; Migliorini, M.; Pourmotabbed, T.; Guha, M.K. Optimization of efficiency in the glyoxalase pathway. *Biochemistry* **1988**, *27*, 7376–7384. [CrossRef]
76. Griffis, C.E.; Ong, L.H.; Buettner, L.; Creighton, D.J. Nonstereospecific substrate usage by glyoxalase I. *Biochemistry* **1983**, *22*, 2945–2951. [CrossRef]
77. Vander Jagt, D.L.; Daub, E.; Krohn, J.A.; Han, L.P. Effects of pH and thiols on the kinetics of yeast glyoxalase I. An evaluation of the random pathway mechanism. *Biochemistry* **1975**, *14*, 3669–3675. [CrossRef]
78. Mullings, K.Y.; Sukdeo, N.; Suttisansanee, U.; Ran, Y.; Honek, J.F. Ni^{2+}-activated glyoxalase I from *Escherichia coli*: Substrate specificity, kinetic isotope effects and evolution within the betaalphabetabetabeta superfamily. *J. Inorg. Biochem.* **2012**, *108*, 133–140. [CrossRef]
79. Rae, C.; O'Donoghue, S.I.; Bubb, W.A.; Kuchel, P.W. Stereospecificity of substrate usage by glyoxalase 1: Nuclear magnetic resonance studies of kinetics and hemithioacetal substrate conformation. *Biochemistry* **1994**, *33*, 3548–3559. [CrossRef]
80. Akoachere, M.; Iozef, R.; Rahlfs, S.; Deponte, M.; Mannervik, B.; Creighton, D.J.; Schirmer, H.; Becker, K. Characterization of the glyoxalases of the malarial parasite *Plasmodium falciparum* and comparison with their human counterparts. *Biol. Chem.* **2005**, *386*, 41–52. [CrossRef]
81. Mannervik, B.; Ridderstrom, M. Catalytic and molecular properties of glyoxalase I. *Biochem. Soc. Trans.* **1993**, *21*, 515–517. [CrossRef]
82. Bergdoll, M.; Eltis, L.D.; Cameron, A.D.; Dumas, P.; Bolin, J.T. All in the family: Structural and evolutionary relationships among three modular proteins with diverse functions and variable assembly. *Protein Sci.* **1998**, *7*, 1661–1670. [CrossRef]
83. Armstrong, R.N. Mechanistic diversity in a metalloenzyme superfamily. *Biochemistry* **2000**, *39*, 13625–13632. [CrossRef]
84. Honek, J.F. Nickel Glyuoxalase I. In *The Biological Chemistry of Nickel*; Kozlowski, H., Zamble, D., Rowinska-Zyrek, M., Eds.; Royal Societ of Chemistry: London, UK, 2017; Volume 10.
85. McCarthy, A.A.; Baker, H.M.; Shewry, S.C.; Patchett, M.L.; Baker, E.N. Crystal structure of methylmalonyl-coenzyme A epimerase from *P. shermanii*: A novel enzymatic function on an ancient metal binding scaffold. *Structure* **2001**, *9*, 637–646. [CrossRef]
86. Dumas, P.; Bergdoll, M.; Cagnon, C.; Masson, J.M. Crystal structure and site-directed mutagenesis of a bleomycin resistance protein and their significance for drug sequestering. *EMBO J.* **1994**, *13*, 2483–2492. [CrossRef]
87. Martin, T.W.; Dauter, Z.; Devedjiev, Y.; Sheffield, P.; Jelen, F.; He, M.; Sherman, D.H.; Otlewski, J.; Derewenda, Z.S.; Derewenda, U. Molecular basis of mitomycin C resistance in streptomyces: Structure and function of the MRD protein. *Structure* **2002**, *10*, 933–942. [CrossRef]
88. Thompson, M.K.; Keithly, M.E.; Harp, J.; Cook, P.D.; Jagessar, K.L.; Sulikowski, G.A.; Armstrong, R.N. Structural and chemical aspects of resistance to the antibiotic fosfomycin conferred by FosB from *Bacillus cereus*. *Biochemistry* **2013**, *52*, 7350–7362. [CrossRef]
89. Gonzalez-Quinonez, N.; Corte-Rodriguez, M.; Alvarez-Fernandez-Garcia, R.; Rioseras, B.; Lopez-Garcia, M.T.; Fernandez-Garcia, G.; Montes-Bayon, M.; Manteca, A.; Yague, P. Cytosolic copper is a major modulator of germination, development and secondary metabolism in *Streptomyces coelicolor*. *Sci. Rep.* **2019**, *9*, 4214. [CrossRef]
90. Aronsson, A.C.; Mannervik, B. Characterization of glyoxalase I purified from pig erythrocytes by affinity chromatography. *Biochem. J.* **1977**, *165*, 503–509. [CrossRef]
91. Mannervik, B.; Lindstrom, L.; Bartfai, T. Partial purification and characterization of glyoxalase I from porcine erythrocytes. *Eur. J. Biochem.* **1972**, *29*, 276–281. [CrossRef]
92. Uotila, L.; Koivusalo, M. Purification and properties of glyoxalase I from sheep liver. *Eur. J. Biochem.* **1975**, *52*, 493–503. [CrossRef]
93. Takatsume, Y.; Izawa, S.; Inoue, Y. Identification of thermostable glyoxalase I in the fission yeast *Schizosaccharomyces pombe*. *Arch. Microbiol.* **2004**, *181*, 371–377. [CrossRef]
94. Sambrook, J.; Russell, D. *Molecular Cloning: A Laboratory Manual*; Cold Spring Harbor Laboratory Press: Cold Spring Harbor, NY, USA, 2001.
95. O'Young, J.; Sukdeo, N.; Honek, J.F. *Escherichia coli* glyoxalase II is a binuclear zinc-dependent metalloenzyme. *Arch. Biochem. Biophys.* **2007**, *459*, 20–26. [CrossRef]

96. Hunt, J.B.; Neece, S.H.; Ginsburg, A. The use of 4-(2-pyridylazo)resorcinol in studies of zinc release from *Escherichia coli* aspartate transcarbamoylase. *Anal. Biochem.* **1985**, *146*, 150–157. [CrossRef]
97. McCall, K.A.; Fierke, C.A. Colorimetric and fluorimetric assays to quantitate micromolar concentrations of transition metals. *Anal. Biochem.* **2000**, *284*, 307–315. [CrossRef]
98. Louis-Jeune, C.; Andrade-Navarro, M.A.; Perez-Iratxeta, C. Prediction of protein secondary structure from circular dichroism using theoretically derived spectra. *Proteins* **2011**, *80*, 374–381. [CrossRef]